89-2200-CP

Method for Simultaneous Wing Aerodynamic and Structural Load Prediction

Mark Drela *
Massachusetts Institute of Technology, Cambridge, Massachusetts

Abstract

A calculation method is presented for the simultaneous solution of aerodynamic and structural loads on arbitrary high aspect ratio wings. The wing aerodynamics are modeled using lifting line theory with roll rate, yaw, and yaw rate effects included. The wing structure is modeled as a nonlinear beam with vertical and horizontal displacement and torsional degrees of freedom. Axial compression effects are also incorporated to permit modeling of wings with external bracing struts or wires. The aerodynamic and structural problems together constitute a coupled nonlinear system for the aerodynamic and structural unknowns, which is discretized and solved using a global Newton method. The overall procedure permits computationally economical prediction of:

1. Aerodynamic and structural loads for a very wide range of operating conditions.
2. Induced drag with static wing twist effects included.
3. Lateral and longitudinal wing static stability derivatives and roll-yaw coupling forces incorporating wing deflections.
4. Static divergence and aileron reversal speeds.
5. Buckling loads for externally braced wings.

Examples are drawn from the wing design of the *Daedalus* human powered aircraft.

Nomenclature

Coordinates and dimensions

b	wingspan
c	local wing chord
j,J	spanwise node index and maximum index
$(x/c)_{sc}$	chordwise shear center location
x,y,z	Cartesian coordinates fixed to aircraft
x,s,n	local coordinates fixed to wing section
s_w	s location of strut or wire attach point
θ	spanwise Glauert coordinate
$\tilde{\vartheta}$	angle of external bracing wire
α	local angle of attack (no loads)

Structural parameters

EA_w	tensile stiffness of external strut or wire
EI_{in}	in-plane bending stiffness
EI_{out}	out-of-plane bending stiffness
EI_{zz}	n deflection bending stiffness
EI_{zn}	x,n deflection bending cross-stiffness
EI_{nn}	x deflection bending stiffness
GJ	torsional stiffness
F_c	point load due to fuselage
F_w	external bracing wire tension

Local structural solution variables

u, w	x,z deflections
φ , ϑ	x,z deflection angles
φ_0,ϑ_0	x,z deflection angles at zero load
t	torsional twist angle
t_0	torsional twist angle at zero load
P	axial tension force
S_x , S_n	x,n shear forces
M_x,M_n	x,n bending moments
T	torsion moment

Global variables and operating parameters

α_∞	overall wing angle of attack
β, $\dot{\beta}$, $\ddot{\beta}$	yaw angle , yaw rate , yaw acceleration
ϕ, $\dot{\phi}$, $\ddot{\phi}$	roll angle, roll rate, roll acceleration
A_n	bound circulation Fourier coefficients

Aerodynamic quantities

a_o	two-dimensional airfoil lift-curve slope
α_i	induced angle of attack
Γ	bound circulation
c_d , c_ℓ	local profile drag and lift coefficient
c_m	local profile pitching moment coefficient
$\mathcal{L}$	total lift
$\mathcal{M}$	total rolling moment
$\mathcal{N}$	total yawing moment
ρ	air density
V , V_∞	local and centerline air velocity

Distributed loads

m_x	moment about x-axis
m_s	moment about local spanwise axis
m_n	moment about local wing-normal axis
p_x	moment about x-axis
p_s	moment about local spanwise axis
p_n	moment about local wing-normal axis
m	wing mass density per unit span
g	gravitational acceleration

*Carl Richard Souderton Assistant Professor, Department of Aeronautics and Astronautics.

1 Introduction

A standard practice in the calculation of wing aerodynamic forces and resulting structural loads involves decoupling the two problems. Some geometry is assumed, typically corresponding to the unloaded wing or some simple assumed deflection mode, and this geometry is then used for aerodynamic force calculations. This is a very effective approach for moderate to low aspect ratios, where the deflections are small and hence have little effect on the aerodynamics. A substantial improvement in accuracy over the decoupled procedure can be obtained by incorporating linearized structural deflections into a linear aerodynamic solution and vice-versa via influence coefficients. An example of this technique is given by Caap and Elmeland [1] for a compact fighter configuration. For very high aspect ratios, however, nonlinear structural theory may be required for sufficient accuracy, especially at limit loads where prediction accuracy is most important. Typical examples are high performance sailplanes, human powered aircraft, and ultralight high-altitude long endurance aircraft. If external bracing at small angles to the wing axis is employed, nonlinear effects can become especially important in load prediction. The *Daedalus* wing is one example where nonlinear effects dominate near limit-load conditions.

A further complication which arises from large structural deflections is that the applied aerodynamic loads are altered nonlinearly. Indeed, in the *Daedalus* , the nonlinear interaction between the static deflection and sideslip is relied on as the sole roll control mechanism! The brute-force approach to solving such a problem would involve iterating repeatedly between the aerodynamic and structural calculations until the overall structural-aerodynamic solution converges. This tends to be an expensive procedure which is not always guaranteed to converge, especially if the structure is near buckling (as in an externally-braced wing). Underrelaxation may be required, which further slows the convergence.

This paper presents a robust and economical procedure for solving the aerodynamic and nonlinear structural problems as a fully-coupled system for a high aspect ratio wing. Lifting line theory governs the spanwise aerodynamic force distributions, and nonlinear bending/torsion beam theory is used to govern the structural response. The structural formulation is assumed static except for rigid-body accelerations. The resulting overall problem for the aerodynamic and structural unknowns is non-linear, but can be readily solved by a global Newton method. Examples are drawn from the *Daedalus* human powered aircraft wing.

2 Structural Formulation

A system of Cartesian coordinates x, y, z is fixed to the aircraft as shown in Figure 1. For a high aspect ratio wing with large deflections, modeling the wing as a nonlinear beam is very accurate. In most actual applications such as the *Daedalus* wing, only the vertical displacements need to

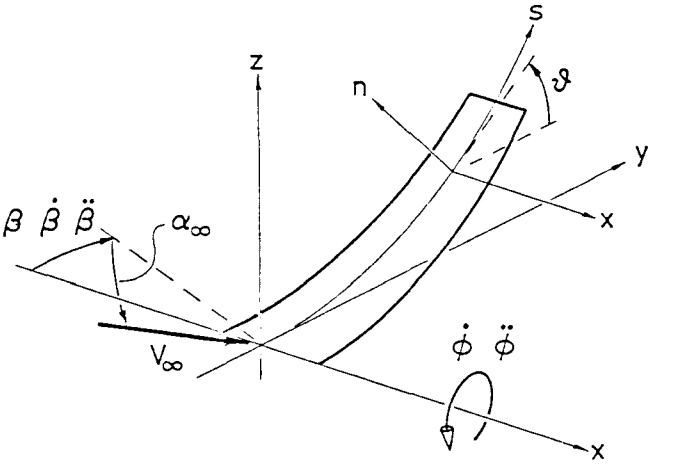

Figure 1: Coordinates and freestream rotation angles.

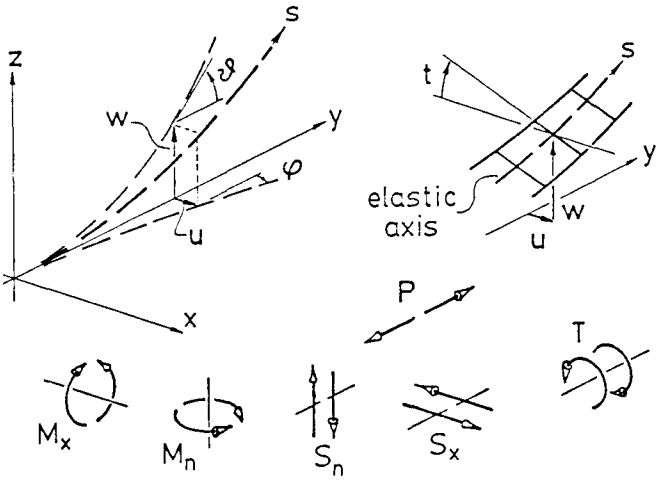

Figure 2: Displacements and structural loads.

be treated nonlinearly, however. It is therefore appropriate to define a local x, s, n coordinate system attached to the wing which undergoes a simple rotation from the Cartesian x, y, z frame by a simple rotation ϑ about the x axis as shown in Figure 1.

Figure 2 shows the sign conventions for the structural displacements u, w of the wing reference axis in the Cartesian frame. The wing reference axis is defined to lie at the shear center location $(x/c)_{sc}$ of each spanwise station. The torsional twist angle t is defined about this reference axis.

The fully nonlinear beam equations as given in Rivello [2] are suitably simplified by assuming the twist angle t to be small, and the fore and aft wing bending deflection u to be small. Only the wing up and down bending deflection w is assumed to be large enough to require non-linear structural analysis. The vertical deflection angle ϑ and the fore and aft deflection angle φ are related to the deflections u and w as follows.

$$\sin\varphi = \frac{du}{ds} \tag{1}$$

$$\sin\vartheta = \frac{dw}{ds} \tag{2}$$

Because even small twist angles can have a significant effect on the aerodynamic loading, torsion effects must be included in the overall analysis. These are generally small enough, however, to permit small-angle simplifications. Similarly, fore and aft deflections can have a substantial effect on the pitching moments of the entire wing as well as affecting the torsion indirectly. For this reason, the fore and aft deflections must be retained even if they are very small. Relation (1) could therefore be safely approximated as $\varphi = du/ds$ although this would not produce a significant computational advantage.

With the wing modeled as a slender beam, only the local bending stiffnesses EI_{xx}, EI_{xn}, EI_{nn}, and the torsional stiffness GJ are needed for a full structural description of the wing. These are defined in the local rotated wing coordinates x, s, n, as are the tension load P, shear loads S, bending moments M, and torsion T.

The beam equilibrium equations in their nonlinear form are given by Rivello [2].

$$\frac{dP}{ds} + S_x\frac{d\varphi}{ds} + S_n\frac{d\vartheta}{ds} + p_s = 0 \tag{3}$$

$$\frac{dS_x}{ds} - P\frac{d\varphi}{ds} + S_n\frac{dt}{ds} - p_x = 0 \tag{4}$$

$$\frac{dS_n}{ds} - P\frac{d\vartheta}{ds} - S_x\frac{dt}{ds} - p_n = 0 \tag{5}$$

$$\frac{dM_x}{ds} - M_n\frac{dt}{ds} + T\frac{d\varphi}{ds} - S_n + m_x = 0 \tag{6}$$

$$\frac{dM_n}{ds} + M_x\frac{dt}{ds} - T\frac{d\vartheta}{ds} - S_x + m_n = 0 \tag{7}$$

$$\frac{dT}{ds} - M_x\frac{d\varphi}{ds} + M_n\frac{d\vartheta}{ds} + m_s = 0 \tag{8}$$

The standard slender beam stress-deflection relations are used to close the equation system, with φ_0, ϑ_0, t_0, denoting the zero load (built-in) deflection angles.

$$M_x = EI_{xn}\frac{d}{ds}(\varphi-\varphi_0) + EI_{xx}\frac{d}{ds}(\vartheta-\vartheta_0) \tag{9}$$

$$M_n = EI_{nn}\frac{d}{ds}(\varphi-\varphi_0) + EI_{xn}\frac{d}{ds}(\vartheta-\vartheta_0) \tag{10}$$

$$T = GJ\frac{d}{ds}(t-t_0) \tag{11}$$

The local section bending stiffnesses EI_{xx}, EI_{xn}, and EI_{nn}, are obtained from the specified in-plane and out-of-plane stiffnesses EI_{in}, EI_{out}. For convenience, these are assumed to be defined in the wing's principal bending axes in which the cross-product stiffness vanishes. The principal axes in the unloaded condition are set at the known angle $\bar{t}$ to the x–y plane. In the *Daedalus* wing, a forward main spar is the only significant torsion and out-of-plane bending member. A small rear spar supplies in-plane bending stiffness only. For this case, the in-plane principal axis goes through both spar centers, and the shear center is located at the main spar as shown in Figure 3. Accounting for the structural

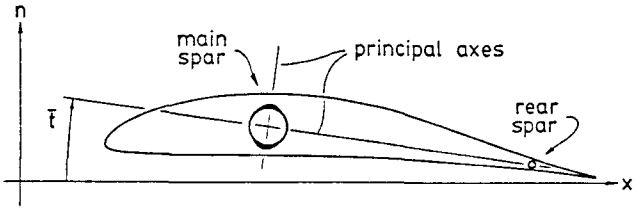

Figure 3: Principal bending axes in the *Daedalus* wing structure.

twist t, the resulting stiffnesses in the s–n frame are given by the following relations.

$$EI_{xx} = EI_{\text{in}}\sin^2(\bar{t}+t) + EI_{\text{out}}\cos^2(\bar{t}+t) \tag{12}$$

$$EI_{xn} = (EI_{\text{out}} - EI_{\text{in}})\sin(\bar{t}+t)\cos(\bar{t}+t) \tag{13}$$

$$EI_{nn} = EI_{\text{in}}\cos^2(\bar{t}+t) + EI_{\text{out}}\sin^2(\bar{t}+t) \tag{14}$$

The force loading functions p_x, p_s, p_n, and moment loading functions m_x, m_s, m_n, arise from distributed wing weight, inertial reactions, aerodynamic forces, and external point loads. Examples of point loads are those due to a fuselage, external stores, or external bracing struts or wires. The *Daedalus* wing employs one lift wire with an angle of $\tilde{\vartheta}$ attached at $s = s_w$ (approximately the midspan). This exerts a force F_w at a point having a small normal offset Δn_w from the spar neutral plane as illustrated in Figure 4. The force is applied directly under the shear center (spar position), so that no applied moment about the s axis results, but the offset Δn_w causes an applied moment about the x axis. The fuselage weight exerts a central point load F_f at $s = 0$. The aerodynamic lift forces are assumed to act at the quarter chord location and normal to the wing's axis and the local relative airflow, with the profile pitching moment coefficient assumed to be constant. The drag forces are taken to act along the relative airflow, whose direction is altered from that of the freestream by the induced downwash angle α_i and roll rate $\dot{\phi}$, which accounts for induced drag and roll-yaw coupling. Both angle corrections are assumed small. The local airspeed is altered from the centerline airspeed via the yaw rate $\dot{\beta}$.

The loading functions for the *Daedalus* wing example are given below, with the point loads represented with the unit impulse function δ.

$$\begin{aligned} p_x &= m\tilde{\beta}s + \frac{1}{2}\rho V^2 c\, c_d \\ &\quad + \rho\left[\dot{\phi}s + V(\alpha_i - \alpha_\infty\cos\vartheta)\right]\Gamma \end{aligned} \tag{15}$$

$$\begin{aligned} p_n &= F_w\sin(\tilde{\vartheta}-\vartheta)\,\delta(s-s_w) - mg\cos\vartheta \\ &\quad - F_f\,\delta(s) - \left(m + \rho\frac{\pi}{4}c^2\right)\tilde{\phi}s + \rho V\Gamma \end{aligned} \tag{16}$$

$$p_s = F_w\cos(\tilde{\vartheta}-\vartheta)\,\delta(s-s_w) - mg\sin\vartheta \tag{17}$$

$$m_x = F_w\cos(\tilde{\vartheta}-\vartheta)\,\delta(s-s_w)\,\Delta n_w \tag{18}$$

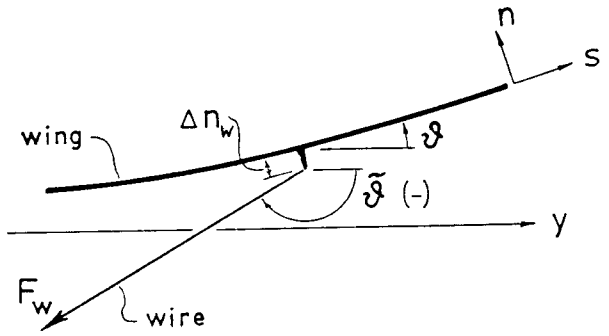

Figure 4: *Daedalus* wing external wire bracing geometry.

$$m_n = 0 \tag{19}$$

$$m_s = \frac{1}{2}\rho V^2 c^2 c_m + \rho V \Gamma c \left[\left(\frac{x}{c}\right)_{sc} - \frac{1}{4}\right] \tag{20}$$

In the case of the *Daedalus* wing, the loading functions depend on the applied forces of the lift wire tension F_w, and the fuselage vertical force F_f. The angle $\tilde{\vartheta}$ of the lift wire in the $y-z$ plane is related to the overall geometry and the wing displacements $w(s_w)$ at the wire attach points (see Figure 4).

$$\cos\tilde{\vartheta} = \frac{s_w}{\sqrt{(h_w + w(s_w))^2 + s_w^2}} \tag{21}$$

The lift wire tension is proportional to its strain which arises directly from the wing displacement at the two lift wire attach points. The wire tension F_w in equations (17), (18), (19) can therefore be expressed in terms of the local deflection $w(s_w)$ by the following stress-strain relation.

$$F_w = EA_w \left(\frac{\sqrt{(h_w + w(s_w))^2 + s_w^2}}{\sqrt{h_w^2 + s_w^2}} - 1 \right) \tag{22}$$

With a first order system of eleven equations, eleven boundary conditions must be imposed to obtain a unique solution. For computational symmetry, however, it is better to treat the two wing halves as two coupled structural problems. A total of twenty-two boundary conditions and compatibility conditions between the two halves are then imposed. At each wingtip ($s = \pm b/2$), zero shear, axial tension, bending moment, and torsion are specified:

$$\begin{aligned}
P(-b/2) &= 0 & P(b/2) &= 0 \\
S_x(-b/2) &= 0 & S_x(b/2) &= 0 \\
S_n(-b/2) &= 0 & S_n(b/2) &= 0 \\
M_x(-b/2) &= 0 & M_x(b/2) &= 0 \\
M_n(-b/2) &= 0 & M_n(b/2) &= 0 \\
T(-b/2) &= 0 & T(b/2) &= 0
\end{aligned} \tag{23}$$

At the wing center, deflections, deflection angles, and twist angles are specified for each wing half.

$$\begin{aligned}
u(-0) &= 0 & u(+0) &= 0 \\
w(-0) &= 0 & w(+0) &= 0
\end{aligned}$$

$$\begin{aligned}
\varphi(-0) &= \varphi_0(-0) & \varphi(+0) &= \varphi_0(+0) \\
\vartheta(-0) &= \vartheta_0(-0) & \vartheta(+0) &= \vartheta_0(+0) \\
t(-0) &= t_0(-0) & t(+0) &= t_0(+0)
\end{aligned} \tag{24}$$

These conditions ensure compatibility between the two wing halves at the centerline. Also, the center point load F_f in equation (17), assumed to be applied at $s = 0$, no longer enters the formulation explicitly. The above conditions assume that the wingroot is clamped. The *Daedalus* wing mount is rather unique in that it is pinned in in roll, and hence can transmit no significant rolling moments into the wing. For this special case, the two constraints on $\vartheta(\pm 0)$ must therefore replaced by conditions of slope and moment continuity.

$$\vartheta(-0) - \vartheta(+0) = \vartheta_0(-0) - \vartheta_0(+0) \tag{25}$$

$$M_x(-0) - M_x(+0) = 0 \tag{26}$$

3 Aerodynamic Formulation

A lifting-line formulation with non-uniform spanwise distribution of the air velocity V is used as the aerodynamic model of the wing. Allowing for the effects of structural twist t, roll rate $\dot{\phi}$, and coupling between sideslip (yaw) β and local dihedral angle $\vartheta = \arcsin(dw/ds)$, the local Γ is given by

$$\begin{aligned}
\Gamma &= \frac{Vc}{2} c_\ell \\
&= \frac{Vc}{2} a_o \left(\alpha + \alpha_\infty \cos\vartheta - \alpha_i + t + \vartheta \sin\beta - \frac{\dot{\phi} y}{V} \right)
\end{aligned} \tag{27}$$

with α being the local angle of attack defined from the local zero-lift line relative to the x axis and with the local twist $t = 0$.

Although the bending deflections were not assumed small in the structural formulation, here the wing is assumed to be flat to permit the application of standard lifting-line theory. This assumption will have a relatively minor effect on the overall aerodynamic solution if the deflections are not too excessive, such as for the *Daedalus* wing examples which will be presented. More exact aerodynamic formulations (such as vortex lattice) could be incorporated to properly account for very large deflections, but at considerably greater computational effort.

With the flat wing assumption, the Cartesian coordinate y in equation (27) can be replaced by the structural spanwise coordinate s. Following standard lifting-line wing theory, this in turn is expressed by the spanwise Glauert coordinate θ.

$$s = \frac{b}{2}\cos\theta \tag{28}$$

This coordinate permits an efficient discretization of Γ as a Fourier series.

$$\Gamma(\theta) = \sum_{n=1}^{\infty} A_n \sin n\theta \tag{29}$$

For computational purposes, the infinite series can be safely truncated to as few as ten terms for most cases. If geometrical discontinuities due to aileron or flap deflection are present, more terms may be required for adequate accuracy. The induced angle corresponding to the bound circulation and associated trailing vorticity is given by

$$\alpha_i(\theta) = \frac{1}{2\,V\,b} \sum_{n=1}^{\infty} n A_n \frac{\sin n\theta}{\sin\theta} \qquad (30)$$

where V is the local air velocity which can have a spanwise variation due to yaw rate.

$$V(\theta) = V_\infty + \dot{\beta}\frac{b}{2}\cos\theta \qquad (31)$$

In terms of the Fourier coefficients, equation (27) becomes the following.

$$\sum_{n=1}^{\infty} A_n \left(\sin\theta + n\frac{c a_o}{4b}\right) \sin n\theta = V\,\frac{c a_o}{2}\left(\alpha + \alpha_\infty \cos\vartheta + t + \vartheta\sin\beta - \frac{\dot{\phi} s}{V}\right)\sin\theta \qquad (32)$$

With the infinite series in equation (32) truncated to N terms, N independent equations for the Fourier coefficients A_n $(n = 1, 2, \ldots, N)$ are obtained through a Fourier decomposition.

$$\begin{aligned} &\int_0^\pi \Big\{\text{equation (32)}\Big\}\ \sin\theta\, d\theta \\ &\int_0^\pi \Big\{\text{equation (32)}\Big\}\ \sin 2\theta\, d\theta \\ &\qquad\vdots \\ &\int_0^\pi \Big\{\text{equation (32)}\Big\}\ \sin N\theta\, d\theta \end{aligned} \qquad (33)$$

These equations depend on the structural twist t and deflection angle ϑ, and hence the Fourier coefficients are coupled to the structural solution, as well as the aircraft angle of attack α_∞, sideslip β, and roll rate $\dot{\phi}$. None of these quantities are known a priori in the general case, where for example only the overall lift or rolling moment, and/or yawing moment may be known or prescribed. Hence, α, β, and $\dot{\phi}$ require additional constraints to fix them. These are readily obtained as appropriately weighted spanwise integrals of the aerodynamic, gravitational, and inertial forces.

$$\mathcal{L} = \int_{-b/2}^{b/2} [-mg + \rho V \Gamma \cos\vartheta]\, ds \qquad (34)$$

$$\mathcal{M} = \int_{-b/2}^{b/2} [-m\ddot{\phi} s + \rho V \Gamma]\, s\, ds \qquad (35)$$

$$\mathcal{N} = \int_{-b/2}^{b/2} \left[m\ddot{\beta} s + \frac{\rho V^2}{2} c_d + \rho(V\alpha_i - \dot{\phi} s)\Gamma\right] s\, ds \qquad (36)$$

The moment definitions (35), (36), use the spanwise arc length coordinate s as the moment arm for the forces at that spanwise location. This is an approximation made for computational simplicity. The associated errors are negligible, since precise knowledge the overall roll and yaw moments is not very important for accurate structural load predictions. The lift can be very important however, and in equation (34) force components are accounted for to second order in the wing deflection. Note that the rolling moment definition (35) includes the inertial reaction from the roll acceleration $\ddot{\phi}$, so that $\mathcal{M}$ as defined will invariably be zero in actual applications (assuming of course that the wing accelerates in roll as a rigid body). External yaw moments can be applied at the wing root with the rudder, however, meaning that $\mathcal{N}$ will not necessarily be zero. The moment definition equations (35), (36) assume that the wing is symmetric in mass distribution. Accounting for non-symmetry would result in only minor complications.

4 Coupled System Solution

The structural problem to be solved is defined by the two displacement-angle relations (1) - (2), the six equilibrium equations (3) - (8), and the three stress-deflection relations (9) - (11). These constitute a first-order system of eleven equations in the eleven unknowns u, w, φ, ϑ, t, P, S_x, S_n, M_x, M_n, T. These unknowns are *local* in the sense that they are functions of the spanwise coordinate s. The first order system also depends on *global* unknowns which appear in the loading functions defined by equations (16) - (21). These are the circulation Fourier coefficients $A_1, A_2, \ldots A_N$, and the global operating parameters α_∞, β, $\dot{\beta}$, $\ddot{\beta}$, $\dot{\phi}$, $\ddot{\phi}$. The N Fourier coefficients are constrained by N equations (33). The applied forces are either specified, or related to the attachment point displacements as in equation (23). The operating parameters are either specified, or implicitly defined by enforcing any number of the three lift and moment relations (34), (35), (36).

4.1 Discretization

The structural problem is discretized using the well-known Keller's Box finite difference scheme [4], which is second-order accurate for arbitrary grid node distributions. The wing is divided into a suitable number of spanwise stations (or grid nodes) at $\theta = \theta_j$, with j being the spanwise index $(-J \le j \le J)$. An ideal distribution for resolving the steep circulation gradients near the wingtips is a uniform node spacing in θ, which produces a "cosine" spacing in the physical spanwise coordinate s. The structural solution, however, dictates a more or less uniform discretization in s. An effective compromise is struck with the following distribution formula for θ_j.

$$\theta_j = \frac{\pi}{2}\left[1 - \frac{1}{2}\left(\frac{j}{J}\right)\left(1 + \frac{|j|}{J}\right)\right] \qquad (37)$$

$$s_j = \frac{b}{2}\cos\theta_j \qquad (38)$$

For a given total number of nodes $2J$, this results in the node spacing at the wing center being reduced by a factor

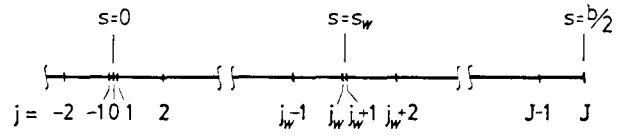

Figure 5: Node indexing.

of 0.5 from the pure cosine spacing. The tip spacing is increased by a factor of 1.5, but still decreases sufficiently towards the tip to properly resolve the circulation gradient.

The node distribution defined by equation (37) is modified slightly to ensure that a node falls wherever a point load is applied. In the case of the *Daedalus* wing, this corresponds to the wing center where the fuselage is attached by a point support, and the station where the lift wire is attached. This index of the latter node is denoted by j_w so that $s_{j_w} = s_w$. Also, the $j_w + 1$ node is placed at the same location, so that $s_{j_w+1} - s_{j_w} = 0$ (see Figure 5). This zero-width interval permits the lift wire load to be introduced as a perfect discontinuity in the shear (for example), with no significant modifications to the finite difference formulas. Likewise, the $j = -1, 0, 1$ nodes all coincide at the centerline for the same reason.

The Keller box differencing scheme applied to the first order structural system results in eleven finite difference equations at each $(j\,,\,j{+}1)$ interval. For example, equation (1) is discretized as

$$\Delta s_{j+\frac{1}{2}} \sin\left(\frac{\varphi_{j+1}+\varphi_j}{2}\right) - u_{j+1} + u_j \equiv R_{u\,j} = 0 \quad (39)$$

where

$$\Delta s_{j+\frac{1}{2}} = s_{j+1} - s_j$$

Note that at the zero-width $(j_w\,,\,j_w{+}1)$ interval for which $\Delta s = 0$, the above equation automatically assumes the correct u-displacement continuity form

$$-u_{j+1} + u_j = 0 \quad (40)$$

with no special treatment. Equation (3), after being combined with the distributed spanwise load definition (18), is discretized as follows.

$$\begin{aligned} &P_{j+1} - P_j \\ &+ \frac{S_{x\,j+1}+S_{xj}}{2}(\varphi_{j+1}-\varphi_j) + \frac{S_{n\,j+1}+S_{nj}}{2}(\vartheta_{j+1}-\vartheta_j) \\ &- \Delta s_{j+\frac{1}{2}} \frac{m_{j+1}+m_j}{2} g \sin\left(\frac{\vartheta_{j+1}+\vartheta_j}{2}\right) \\ &+ F_w \cos\left(\tilde{\vartheta} - \frac{\vartheta_{j+1}+\vartheta_j}{2}\right) \delta_{j\,,\,j_w} \equiv R_{P\,j} = 0 \end{aligned} \quad (41)$$

In the above equation, the wire angle $\tilde{\vartheta}$ and tension F_w are defined in terms of ϑ_{j_w} by relations (22) and (23). Also, the product $\Delta s\,\delta(s{-}s_w)$ has been replaced by the Kronecker delta, defined as

$$\delta_{j\,,\,j_w} = \begin{cases} 1 & \text{if } j = j_w \\ 0 & \text{if } j \neq j_w \end{cases} \quad (42)$$

Note that for the zero-width $(j_w\,,\,j_w+1)$ interval where the lift wire is attached, equation (41) automatically reverts to

$$P_{j_w+1} - P_{j_w} = -F_w \cos\left(\tilde{\vartheta} - \vartheta_{j_w}\right) \quad (43)$$

which simply causes the axial load P of the wing to correctly jump by an amount equal to the axial load applied by the wire. Again, no special differencing form is required at this interval. As a final example, equation (5) is discretized as follows.

$$\begin{aligned} &S_{n\,j+1} - S_{n\,j} \\ &- \frac{P_{j+1}+P_j}{2}(\varphi_{j+1}-\varphi_j) + \frac{S_{x\,j+1}+S_{xj}}{2}(t_{j+1}-t_j) \\ &- \Delta s_{j+\frac{1}{2}}\,\rho\left(V_\infty + \dot{\phi}\,\frac{s_{j+1}+s_j}{2}\right)\sum_n A_n \sin n\theta \\ &- \Delta s_{j+\frac{1}{2}} \frac{m_{j+1}+m_j}{2} g \sin\left(\frac{\vartheta_{j+1}+\vartheta_j}{2}\right) \\ &+ F_w \sin\left(\tilde{\vartheta} - \frac{\vartheta_{j+1}+\vartheta_j}{2}\right)\delta_{j,j_w} \equiv R_{S\,j} = 0 \end{aligned} \quad (44)$$

Again, for the zero-width $(j_w\,,\,j_w+1)$ interval, equation (44) automatically reverts to

$$S_{n\,j+1} - S_{n\,j} = -F_w \sin\left(\tilde{\vartheta} - \vartheta_{j_w}\right) \quad (45)$$

which gives the correct jump in the shear S_n due to the normal lift wire load component.

The equations (33) which constrain the Fourier circulation coefficients are put into discrete form by simple trapezoidal summation.

$$\begin{aligned} &\sum_{j=-J}^{J-1} \sin\theta_{j+\frac{1}{2}}\,\Delta\theta_{j+\frac{1}{2}} \\ &\quad \left\{ \sum_n A_n \left(\sin\theta + n\frac{ca_o}{4b}\right)_{j+\frac{1}{2}} \sin n\theta_{j+\frac{1}{2}} \right. \\ &\quad - \left[V\frac{ca_o}{2}\left(\alpha + \alpha_\infty \cos\varphi \right.\right. \\ &\qquad \left.\left. + t + \vartheta \sin\beta - \frac{s\dot{\phi}}{V}\right)\sin\theta \right]_{j+\frac{1}{2}} \Bigg\} \\ &\qquad \equiv R_{An} = 0 \end{aligned} \quad (46)$$

where the subscript $j+\frac{1}{2}$ implies an average between $j+1$ and j.

$$\left(\ \right)_{j+\frac{1}{2}} = \frac{(\ )_{j+1} + (\ )_j}{2}$$

4.2 Newton System

The nonlinear system to be solved has the form

$$\mathbf{R(U)} = \mathbf{0} \quad (47)$$

where $\mathbf{U}$ is the unknown vector whose components consist of all the local structural unknowns, and global aerodynamic unknowns. $\mathbf{R}$ is a vector function whose components consist of local finite-difference residual functions such as

$R_{u\,j}$, $R_{P\,j}$, or $R_{S\,j}$ as defined by equations (39), (41), (44), or discretized global constraint residuals such as R_{An} as defined by equation (46). Given an approximate solution $\mathbf{U}^\nu$ at iteration level ν, the change $\delta\mathbf{U}$ needed to obtain an improved guess $\mathbf{U}^{\nu+1}$ is determined by solving exactly the linearized form of (47)

$$\left[\frac{\partial \mathbf{R}}{\partial \mathbf{U}}\right]^\nu \delta\mathbf{U} = -\mathbf{R}^\nu \qquad (48)$$

$$\mathbf{U}^{\nu+1} = \mathbf{U}^\nu + \delta\mathbf{U} \qquad (49)$$

which drives the residual vector $\mathbf{R}$ closer to zero. The known Jacobian matrix $\partial\mathbf{R}/\partial\mathbf{U}$ in equation (48) consists of a block tridiagonal matrix with $2J$ rows of 11×11 blocks filled with partial derivatives of the structural residual functions such as (44)

$$R_{S\,j}(\varphi_j\,,\vartheta_j\,,t_j\,,P_j\,,S_{x\,j}\,,S_{n\,j}\,,\\ \varphi_{j+1}\,,\vartheta_{j+1}\,,t_{j+1}\,,P_{j+1}\,,S_{x\,j+1}\,,S_{n\,j+1}\,,\\ A_1\,,A_2\,,\ldots A_N\,,\dot\phi\,)$$

evaluated with the current approximate solution. Each block row also contains a number of full columns corresponding to the global variables, since $R_{S\,j}$ also depends on the global variables $A_1\,, A_2\,, \ldots A_N\,, \dot\phi$. The Jacobian matrix also contains an additional small number of rows (one for each global variable) corresponding to the linearized global constraint functions such as

$$R_{An}(\vartheta_{-J}\,,t_{-J}\,,\vartheta_{-J+1}\,,t_{-J+1}\,,\ldots,\vartheta_J\,,t_J\,,\\ A_1\,,A_2\,,\ldots,A_N\,,\alpha_\infty\,,\beta\,,\dot\beta\,,\dot\phi\,)$$

which is given fully by equation (33). However, since R_{An} depends on structural variables at all spanwise stations, these rows are generally full. This precludes solving the linear Newton system (48) by a standard block-elimination algorithm. To simplify the overall solution procedure, the Newton system is split into two systems — a large, sparse, strictly block-triagonal system for the changes in the local structural unknowns $\delta\mathbf{U}_\ell$, and a relatively small, generally full system for the changes in the global aerodynamic unknowns and operating parameters $\delta\mathbf{U}_g$.

$$\left[\frac{\partial \mathbf{R}_\ell}{\partial \mathbf{U}_\ell}\right]^\nu \delta\mathbf{U}_\ell = -\mathbf{R}_\ell^\nu - \left[\frac{\partial \mathbf{R}_\ell}{\partial \mathbf{U}_g}\right]^\nu \delta\mathbf{U}_g \qquad (50)$$

$$\left[\frac{\partial \mathbf{R}_g}{\partial \mathbf{U}_g}\right]^\nu \delta\mathbf{U}_g = -\mathbf{R}_g^\nu - \left[\frac{\partial \mathbf{R}_g}{\partial \mathbf{U}_\ell}\right]^\nu \delta\mathbf{U}_\ell \qquad (51)$$

Equation (50) with the multiple righthand sides is readily solved by a standard block elimination method to give

$$\delta\mathbf{U}_\ell = -\mathbf{r} - \left[\,\bar{\bar{\mathbf{s}}}\,\right]\delta\mathbf{U}_g \qquad (52)$$

which is substituted into (51) to produce

$$\left[\frac{\partial \mathbf{R}_g}{\partial \mathbf{U}_g} - \frac{\partial \mathbf{R}_g}{\partial \mathbf{U}_\ell}\,\bar{\bar{\mathbf{s}}}\right]^\nu \delta\mathbf{U}_g = -\mathbf{R}_g^\nu + \left[\frac{\partial \mathbf{R}_g}{\partial \mathbf{U}_\ell}\right]^\nu \mathbf{r} \qquad (53)$$

which is a full but relatively small system involving only the global unknown changes $\delta\mathbf{U}_g$, and is easily solved by Gaussian elimination. By substituting the now known global variable changes into the partially determined system (52), the local variable changes $\delta\mathbf{U}_g$ are completely determined. The local and global solution can now be updated,

$$\mathbf{U}_\ell^{\nu+1} = \mathbf{U}_\ell^\nu + \delta\mathbf{U}_\ell \qquad \mathbf{U}_g^{\nu+1} = \mathbf{U}_g^\nu + \delta\mathbf{U}_g \qquad (54)$$

and the overall process repeated if the changes are above a convergence tolerance. For the *Daedalus* wing in level flight conditions, about three Newton iterations are required to converge to machine accuracy. If the solution is close to a structural instability, however, as many as eight iterations may be required.

5 Validation and Applications

The complexity and degree of generality of the present method makes thorough validation of the theoretical formulation and the computational implementation quite difficult. Limiting problems for which analytic solutions are available can be calculated to validate the bulk of the implementation. A further test of the overall coupled structural/aerodynamic formulation results from comparisons with structural measurements of the *Daedalus* wing under load.

5.1 Elliptically-loaded wing

If the following simplifications are made, an analytically tractable aerodynamic/structural problem results:

1. Deflections and structural twists are made small by specifying $EI_{\rm in}, EI_{\rm out}, GJ \gg \mathcal{L}\,b^2$, $mg = 0$.
2. The external loads and spar compression are zero $F_w = P = 0$.
3. The wing has no twist (α = constant) and has an elliptical planform $c = c_o \sin\theta$.
4. Yaw and roll angles, rates, and accelerations are zero $\beta = \dot\beta = \ddot\beta = 0$, $\phi = \dot\phi = \ddot\phi = 0$.
5. Nonuniform bending stiffnesses of the form $EI \sim \sin\theta$ are chosen.

The latter assumption also tests the representation of a non-uniform beam.

According to classical lifting-line theory, a wing with an elliptic planform and no twist experiences an elliptic spanwise circulation distribution $\Gamma = A_1 \sin\theta$. The first harmonic coefficient is given by

$$A_1 = \frac{1}{2}c_o V \frac{a_o}{1+\frac{a_o c_o}{4b}}\alpha \qquad (55)$$

and all higher harmonics are zero. By specifying a zero wing mass distribution, excluding all point loads and acceleration effects, and assuming negligible induced drag (high aspect ratio), the only loading function is

$$p_n = \rho V_\infty A_1 \sin\theta = p_o \sin\theta \qquad (56)$$

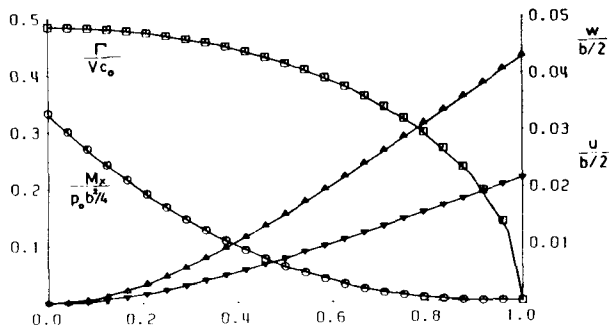

Figure 6: Test comparison of computed (lines) and analytic (symbols) solution for high aspect ratio elliptical wing.

for which an analytic solution can be obtained for all the structural variables.

Figure 6 compares the computed circulation distribution Γ, bending moment M_x, and deflections u and w with the analytical solution for a high aspect ratio ($b/c_o = 100$) elliptical wing for which all the above assumptions hold. The in-plane and out-of-plane bending stiffnesses were chosen so that $EI_{\text{in}} = 3EI_{\text{out}}$, and the wing's local principal bending axis angle was specified to be at $\bar{t} = 45^o$ to the $x - y$ plane. This tests the implementation of the local stiffness relations (12 - 14) and the cross-coupling in the moment-deflection relations (9 - 10). Despite the relatively small number of points ($J = 11$), the solutions match perfectly. Since the aerodynamic formulation determines the beam loading and the structural formulation determines the resulting structural moments and deflections, both formulations are checked for correctness in this test. The computation time required for this case was 5s CPU on a MicroVax II.

5.2 *Daedalus* wing — level flight

The present calculation method was extensively employed in the wing design for the *Daedalus* human powered aircraft. The actual planform and structural parameters of this wing are shown in Figure 7. The parameter discontinuities are due to stepping of the graphite-epoxy plys in the main spar. The wing's overall aspect ratio is 38, making it an ideal application for the present method.

Figure 8 shows the computed loading, shear, and moment distributions on the wing in level flight. A typical airspeed of 22 ft/s and a gross weight of 240 lb were specified for this case, and the corresponding overall angle of attack α_∞ was automatically determined by the global Newton solution scheme. Also shown is a photograph of the aircraft in flight under these operating conditions. The calculated and observed wing deflection shapes agree perfectly within plotting accuracy. Note that the structural load discontinuities due to the wire and fuselage loads are captured exactly as discussed previously. This calculation was performed with $J = 51$ points on each wing half, and $N = 11$ circulation

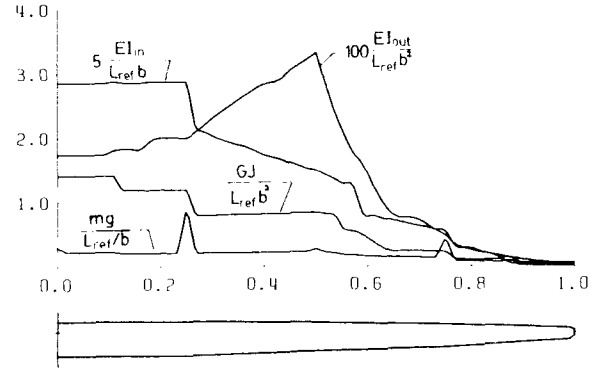

Figure 7: Planform and structural parameters of the *Daedalus* wing. $L_{\text{ref}} = 230$ lb.

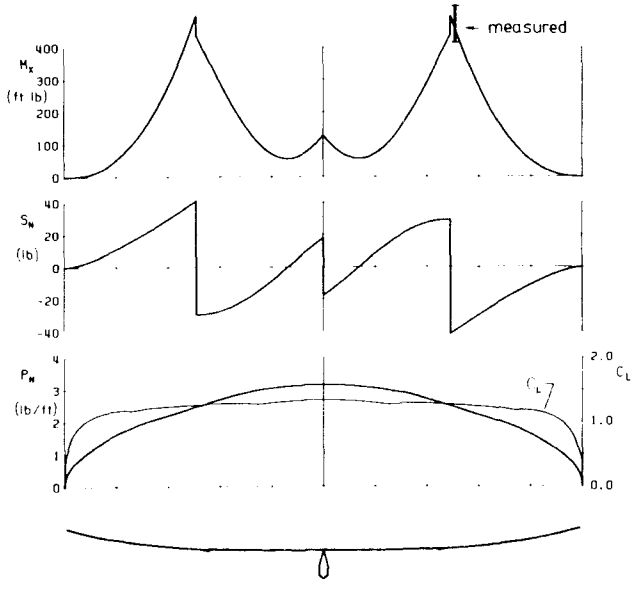

Figure 9: Calculated structural loads on the *Light Eagle* wing in level flight, with measured bending moment range.

harmonics. Three Newton iterations were required with a total of 60 s CPU time.

In-flight strain gauge measurements were taken on the *Light Eagle* aircraft which served as a prototype for the *Daedalus* . Figure 9 shows the bending moment distribution with the range of values measured just outboard of the wire attachment points. The strain gauges were calibrated by directly applying known bending moments to the wing in the hangar. A 10 Hz data sampling rate used over a flight period of several minutes gave a large number of quite reliable data points. The spread in the measurements is apparently caused mainly by gust loads. The mean measured moment compares quite well with the calculation.

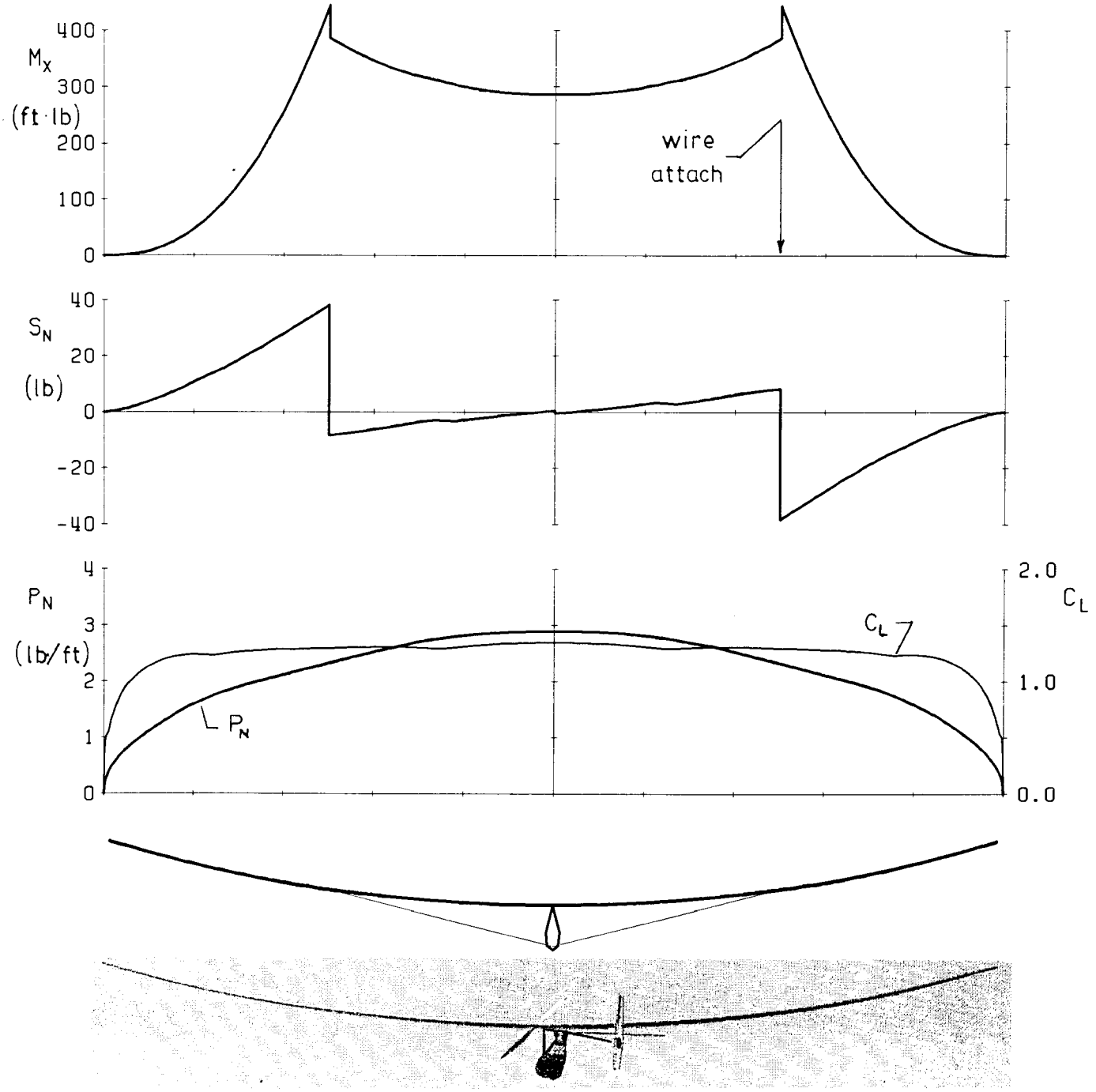

Figure 8: Calculated structural loads on the *Daedalus* wing in level flight, with photograph of actual aircraft.

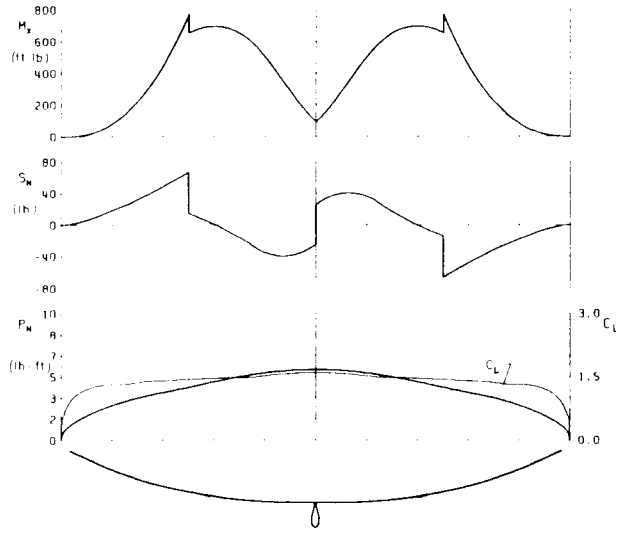

Figure 10: Calculated structural loads on the *Daedalus* wing in a 1.8-g pullup.

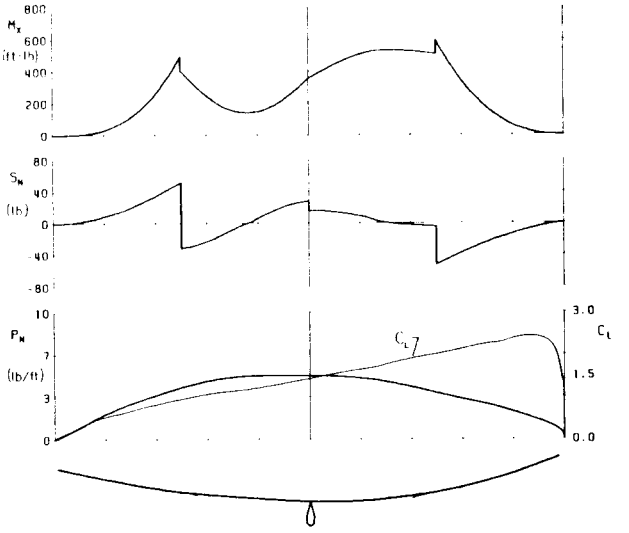

Figure 11: Calculated structural loads on the *Daedalus* wing in a 1.6-g pullup with a 30° sideslip angle.

5.3 High-lift and Maneuvering Loads

Due to very strong pitch damping and a cruise lift coefficient close to stall, it is nearly impossible to exceed 1.1 g's on the *Daedalus* with full stick deflections, as the *Light Eagle* flight tests have shown [5]. Nevertheless, the wing must be stressed to higher g-loads since gusts, higher speeds, and slipping maneuvers greatly aggravate the situation.

The *Daedalus* wing was nominally stressed to 1.8 g's [6]. A straight-pullup calculation, with the normal level-flight lift and the wing mass distribution both multiplied by the 1.8 load factor, is shown in Figure 10. A relatively high airspeed of 28 ft/s is specified to avoid unrealistically high lift coefficients. The wing is in no danger of buckling, although material stresses are just exceeded in the wing spar.

In Figure 11, a $\beta = 30°$ sideslip is combined with a 1.6-g pullup. Such seemingly extreme sideslip angles were actually measured on the *LightEagle* aircraft which was equipped with an air data system. This maneuver is representative of a "panic recovery" from an imminent spiral dive — not an infrequent occurrence in human powered aircraft. The wing has nearly snapped through on the right wing (yawed into the airstream), with the attendant bending moment increases. Specifying a load factor of 1.65 g's results in failure of the Newton algorithm to converge, indicating buckling. This shows the dramatic effects on the load margin which can result from unfavorable flight attitude combinations. It must be stressed that the nonlinear fully-coupled formulation of the present analysis is essential to capture this behavior, and was crucial in the structural design of the Daedalus wing for actual flight conditions.

It is important to point out that in addition to the sideslip β, the calculated loads can be quite sensitive to the particular values of yaw rate $\dot{\beta}$ and roll rate $\dot{\phi}$ selected. For the above case, a zero roll rate $\dot{\phi} = 0$ was specified, and the yaw rate $\dot{\beta}$ was implicitly determined by specifying a zero net rolling moment $\mathcal{M}$ with equation (35). This corresponds to a steady-state turn with the constant sideslip β overcoming the inward rolling moment due to the yaw rate. Equivalently, a zero yaw rate $\dot{\beta}$ could be specified, and the roll rate $\dot{\phi}$ determined as a result. This flexibility is very valuable in quickly investigating various flight situations to determine the likeliest failure scenario. For any flight situation, aerodynamic performance values such as induced drag are also determined, allowing the estimation of drag penalties from maneuvering flight.

5.4 Divergence speed

The current method is capable of estimating the speed at which structural divergence occurs. Figure 12 shows the structural solution of the *Daedalus* wing for the rather high speed of 45 ft/s. The wing is very severely twisted due to the airfoil pitching moment, and the wing tips are close to "tuck-in". If a flight speed of 48 ft/s is specified, the Newton algorithm refuses to converge, indicating divergence. For this particular aircraft, this divergence speed could only be achieved with an unreasonably steep dive.

A very similar approach could be used to determine aileron reversal speeds. The effect of an aileron is incorporated by a modification of the local aerodynamic angle α and pitching moment coefficient c_m. By monitoring the net rolling moment on the aircraft, it is a simple matter to determine the reversal airspeed at which the structural twist t over the entire wing caused by the additional aileron pitching moment overcomes the effective addition to α at

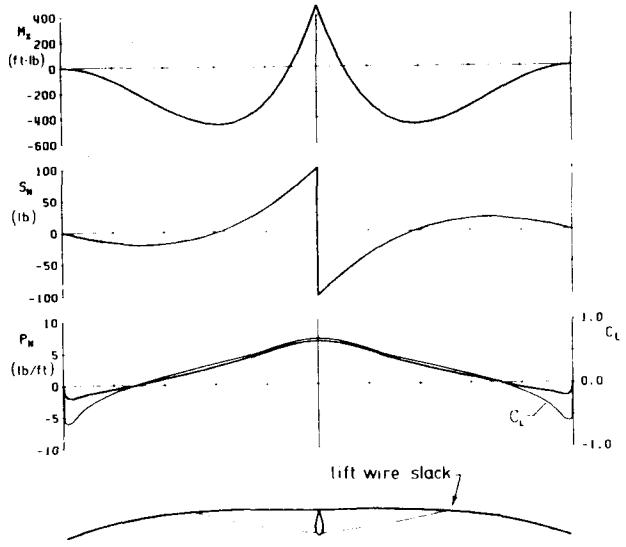

Figure 12: Calculated structural loads on the *Daedalus* wing near divergence speed.

the aileron location.

6 Conclusions

A method for the simultaneous calculation of aerodynamic and structural loads has been developed and applied to the design and analysis of a flexible high aspect ratio wing. The strong coupling between static deflections and aerodynamic loads has been treated by solving the entire nonlinear aerodynamic/structural equation set as a fully-coupled system by a global Newton method. The overall scheme is very accurate, robust, and computationally economical.

Calculated examples illustrated the versatility of this numerical tool for the prediction of structural loads for design and limit loads, and the determination of lateral stabiiity derivatives and aerodynamic performance in the presence of large static deflections. Flight modes which include any combination of roll and yaw angles, angle rates, and angular accelerations can also be simulated to determine loads and aerodynamic performance under these conditions.

Although the present method is applicable to any moderate to high aspect ratio wing, it is especially valuable in relatively flexible aircraft. Applications for which the present method is particularly well suited include human powered aircraft, very high altitude remotely piloted vehicles, and high performance sailplanes.

Acknowledgements

This research was supported by the MIT Dean of Engineering Office.

References

[1] Caap, P., and Elmeland, L., "Calculation of Static Elastic Effects on a Modern High Performance Fighter Aircraft," AIAA-86-1771-CP presented at the AIAA 4th Applied Aerodynamics Conference, June 1986.

[2] Rivello, R. M., *Theory and Analysis of Flight Structures*, McGraw-Hill, 1969.

[3] Bussolari, S. R., Langford, J. S., and Youngren, H. H., "Flight Research with the MIT Daedalus Prototype," presented at the SAE Aircraft Design and Testing Conference, St. Louis, MO, June 1987.

[4] Keller, H. B., "Accurate Numerical Methods for Boundary Layer Flows: I. Two Dimensional Laminar Flows," *Proceedings of the Second International Conference on Numerical Methods in Fluid Dynamics*, von Karman Institute for Fluid Dynamics, Sept. 1970.

[5] Sullivan, R. B., and Zerweckh, S. H., "Flight Test Results for the Daedalus and Light Eagle Powered Aircraft," MIT Aero. & Astro. Dept. Report, Cambridge, MA, 1988.

[6] Cruz, J. R. "Structural Design Conditions and Load Determination for Human Powered Aircraft," 21st OSTIV Conference, Wiener Neustadt, Austria.